Proceedings of the ASME 2019 38th International Conference on Ocean, Offshore and Arctic Engineering
OMAE2019
June 9-14, 2019, Glasgow, Scotland, UK

OMAE2019-96680

NUMERICAL SIMULATION OF FULLY NONLINEAR INTERACTION BETWEEN REGULAR AND IRREGULAR WAVES AND A 2D FLOATING BODY

Haoran Li[1] , Erin. E. Bachynski
Department of Marine Technology, Norwegian University of Science and Technology
Trondheim, Norway

ABSTRACT

A fully nonlinear Navier-Stokes/VOF numerical wave tank, developed within the open-source CFD toolbox OpenFOAM, is used to investigate the response of a moored 2D floating body to nonlinear wave loads. The waveDyMFoam solver, developed by extending the interDyMFoam solver of the OpenFOAM library with the waves2Foam package, is applied. Furthermore, a simple linear spring is implemented to constrain the body motion. An efficient domain decomposition strategy is applied to reduce the computational time of irregular wave cases. The numerical results are compared against the results from potential flow theory. Numerical results highlight the coupling between surge and pitch motion and the presence of nonlinear loads and responses. Some minor numerical disturbance occurs when the maximum body motion response is achieved.

Keywords: flow-induced motion, flow-induced load, WaveDyMFoam, OpenFOAM

INTRODUCTION

Floating wind turbines may be exposed to very harsh environments and extremely steep waves which induce large motions. As a result, there is increasing interest in investigating interactions between nonlinear waves and floating structures by various simulation tools [1,2]. In general, two classes of numerical methods are implemented. One is based on potential flow theory. Another one is based on solving the Navier-Stokes equations together with proper boundary conditions.

For the potential flow theory, it is typically assumed that the water is incompressible, irrotational and inviscid. One of the most well-known tools is the WAMIT software, developed by Lee and Newman [3]. Furthermore, fully nonlinear potential flow models based on boundary element method [4-6] or finite element method [7,8] are developed by many researchers to deal with two-dimensional and three-dimensional wave-body interaction problems. Although the potential flow models can predict the global wave pattern, they cannot model breaking-waves and problem in which extreme nonlinearities and eddies take place.

Strongly nonlinear problems require the use of fully nonlinear viscous numerical models. These are computationally more expensive, but with the development of computational power, are becoming more feasible. For example, the heave performance of a two-body floating-point absorber wave energy system has been simulated based on Reynolds-averaged Navier-Stokes equations [9]. The response of a moored floating body under regular waves has been analyzed using computational fluid dynamics (CFD) [10]. Most studies focus on the regular wave-body interaction problem, not considering the irregular wave-body interaction due to higher computational time. Moreover, comparisons between potential flow and CFD are presented in [11]. The general conclusion is that nonlinear effects such as viscous drag and nonlinear wave loading have a large effect on the body motions and loads, and numerical models should take this into account.

The aim of this paper is to build a well validated fully nonlinear wave tank for the accurate simulation of regular and irregular wave-body interaction using higher order model based on the open-source CFD-toolbox OpenFOAM [12]. In future work, this numerical wave tank will be used for analyzing the response of semi-submersible offshore floating wind turbines under harsh wave conditions.

[1] Contact author: haoran.li@ntnu.no

1.Methods

OpenFOAM [12] is an efficient tool for numerical solution of fluid-structure interaction problems. The multiphase interDyMFoam solver is a fully nonlinear Navier-Stokes/VOF solver used for the accurate simulation of complex free surface flows and fluid-structure interaction, where the flow-dependent motions of rigid bodies are obtained by combining with a 6-DOF dynamic motion solver. The waveDyMFoam solver, based on interDyMFoam solver, was extended with the implementation of the wave generation and absorption toolbox, waves2Foam, developed by Jacobsen et al [13]. Meanwhile, an implementation for the restraints of floating bodies was developed. Furthermore, a fully nonlinear potential flow solver, Oceanwave3D [14], coupled with a fully nonlinear Navier-stokes/VOF solver is applied to reduce the computational time for irregular wave case.

1.1 GOVERNING EQUATIONS

The waveDyMFoam solver utilizes the two-phase incompressible Navier-Stokes equations combined with a VOF-surface capturing scheme [15] to compute fluid-structure interactions. The governing equations are described by the conservation of mass and momentum of an incompressible flow of air and water and are expressed in their differential form:

$$\nabla \cdot \mathbf{u} = 0 \tag{1}$$

$$\frac{\partial \rho \mathbf{u}}{\partial t} + \nabla \cdot (\rho \mathbf{u})\mathbf{u}^T = -\nabla p^* + (\mathbf{g} \cdot \mathbf{x})\nabla \rho + \nabla \cdot \mu \nabla \mathbf{u} \tag{2}$$

where $\nabla = (\partial_x, \partial_y, \partial_z)$ is the three-dimensional gradient operator, $\mathbf{u} = (u, v, w)$ is the velocity field in the Cartesian coordinates, $\mathbf{g}$ is the vector acceleration due to gravity, μ is the dynamic viscosity and p^* is the pressure in excess of the hydrostatic pressure, which is related to the total pressure by

$$p = p^* + \rho(\mathbf{g} \cdot \mathbf{x}). \tag{3}$$

Furthermore, the local density ρ, and the viscosity μ, defined in terms of the water and air volume fraction α, are formulated as:

$$\rho = \alpha \rho_{water} + (1-\alpha)\rho_{air} \tag{4}$$

$$\mu = \alpha \mu_{water} + (1-\alpha)\mu_{air} \tag{5}$$

Where α is one for water, zero for air and in between zero and one for all intermediate values.

This field is advanced in time once the velocity is solved by Equation (1) and (2), following the modified transported equation,

$$\frac{\partial \alpha}{\partial t} + \nabla \cdot \mathbf{u}\alpha + \nabla \cdot \mathbf{u}_r \alpha(1-\alpha) = 0 \tag{6}$$

Using a standard finite-volume approximation for solving Equation (6) will lead to significant smearing of the interface. This can be reduced by introducing the additional convective term [16]. It is governed by $\mathbf{u}_r$, an artificial velocity field normal to and pointing towards the free surface. It only exists in the vicinity of the interface, $0 < \alpha < 1$. Even though its magnitude is proportional to the instantaneous velocity, it lacks any physical meaning. To ensure the stability of solution, a multi-dimensional flux limited scheme (MULES) is applied to solve the Equation (6).

To identify the free surface elevation, wave gauges in the waves2Foam package are applied. The wave gauges are placed at certain positions in the numerical domain, so that the free surface elevation ζ, relative to the still water level, is given by:

$$\zeta = \int_{x_0}^{x_1} \alpha dz - d \tag{7}$$

where x_0 and x_1 are the user-defined start and end points in the vertical line over which the α field is integrated, and d is the initial water depth for still water.

1.2 BOUNDARY CONDITIONS

To solve the governing equations of the Navier-Stokes/VOF solver, boundary conditions are imposed to all surfaces in the numerical domain. The general denomination of boundary surfaces is given in Figure 1.

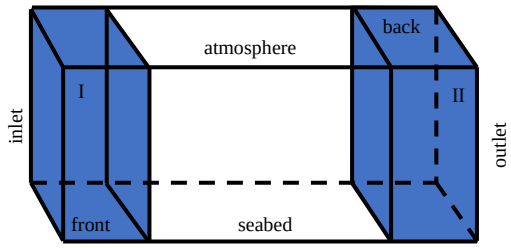

FIGURE 1: SCHEMATIC REPRESENTATION OF COMPUTATIONAL DOMAIN, WHERE I AND II ARE RELAXATION ZONES.

The velocity and the α field boundary conditions at the inlet and outlet surfaces are given by the analytic wave theory. In this paper, a stream function wave theory is applied. At the body surface, a slip condition is applied, which means the viscous boundary layer near the body is not resolved. However, the governing equations still contain the effect of viscosity and turbulence generation due to internal stresses and the free surface motion near the structure. At the seabed, a slip condition is applied. For the two-dimensional simulation in this paper, an empty condition is applied to the front and back walls. This implies that no solution is required at these walls. At the atmosphere boundary, the total pressure is set to zero and an atmospheric boundary condition is applied for the velocity and α field. This means that air and water are allowed to leave the numerical domain, while only air is allowed to flow back in.

The relaxation zones in the waves2Foam toolbox [13] are implemented to avoid wave reflection from outlet boundary and

also to prevent internally reflected waves. An arbitrary shape of relaxation zone can be defined. In this paper, rectangular relaxation zones are used. See Bruinsma's work [17] for a more detailed description of this particular relaxation zone set-up.

1.3 SPATIAL AND TEMPORAL DISCRETIZATION

The numerical wave tank is formed as a box domain which is created with the *blockMesh* utility provided by OpenFOAM and the *snappyHexMesh* utility is used to sculpt the surface boundary of body inside the mesh, where 2-2 level of refinement is used. The local refinement allows for a high-resolution interface while keeping the total number of computational cells relatively low. The spatial discretization of the numerical domain is based on the cell size outside the refinement zone, which is defined by the number of points per structure length (p.p.s.l) as,

$$\Delta = \frac{L}{p.p.s.l} \tag{8}$$

where L is the length of numerical domain. The cell size next to the body surface boundary is 4 times smaller than Δ.

In order to ensure numerical stability, the Courant-Friedrichs-Lewy (CFL) condition is used to determine the time step of numerical simulation. Throughout the paper, the maximum Courant number is set to 0.25. For the regular wave case, a variable time step is set to reduce time-consumption, while a fixed time step (0.0005 s) is used in irregular waves for the convenience of post-processing.

1.4 COUPLING OF NAVIER-STOKES/6DOF SOLVER

In order to simulate flow-dependent motion of a floating body, the Navier-Stokes/VOF solver must be coupled with a six-degrees of freedom motion solver.

The acceleration, velocity and displacement of a floating body are calculated based on the forces and moments on the body. The total forces and moments at the center of mass of body come from the action of fluid and other external forces, such as gravity force and restraining forces. The flow-induced loads on the body are determined by integrating the pressures obtained by solving Equations (1) and (2) along the wetted body surface.

Once the motion of the body is determined, it is necessary to move the body boundary and the mesh surrounding it. Two different approaches can be used to handle this problem. The first one allows for the topological changes, which implies that the number of points, faces and cells in the mesh can vary to comply with the motion of body. The second one allows the mesh to deform while the number of faces, points and cells remain constant. The latter of the two is applied in the waveDyMFoam solver. A thorough discussion on the implementation of deformation algorithm, the radial basis function interpolation, can be found in the work of Bos et al [18].

For a numerical model with a weak coupling between Navier-Stokes/VOF solver and 6-DOF motion solver, the existence of artificial added mass will change the behavior of the body and induce instability. This phenomenon is thoroughly discussed in the work from Causin et al. [19] and Dubar et al. [20]. Hence, a strong coupling between two solvers was established to improve the stability of numerical model. One option is the under-relaxation method [21]. An under-relaxation factor is applied to the acceleration of body. Another approach is the predictor-corrector method [20]. Both two methods have already been implemented in this paper.

The restraints for the moving body in this paper are implemented by a linear spring which is given a simple constant stiffness and a rest length. The force in the spring follows Hooke's law. The spring is defined such that the force is equal to zero when the length of spring is equal to the rest length.

1.5 COUPLING OF NAVIER-STOKES/POTENTIAL-FLOW SOLVER

In order to minimize numerical diffusion and reduce the computational time, a domain decomposition strategy is applied. This strategy is based on one-way coupling, where the information only propagates from outer domain to inner domain. As illustrated in Figure 2, the numerical domain is split into an inner domain where the Navier-Stokes/VOF equations are solved, to accurately simulate wave-structure interactions, and an outer domain where the potential flow equations are used for the time efficient simulation of realistic sea states. The smaller CFD domain, Γ ,is located inside the larger potential flow domain Ω. Two wave generation and absorption zones, I and II, are utilized in the potential flow solver. The domains are coupled by generalized coupling zones of arbitrary shapes. Throughout this paper, the coupling zones are the relaxation zones provided by the waves2Foam toolbox. The one-way coupling of waveDyMFoam solver with Oceanwave3D, a fully nonlinear three-dimensional potential solver developed by Engsig-Karup et al. [22], is used in this paper. More details about this coupling can be found in the work of Paulsen et al. [23].

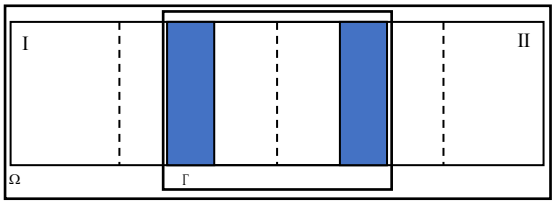

FIGURE 2: SCHEMATIC REPRESENTATION OF THE DOMAIN OF THE POTENTIAL FLOW SOLVER, Ω ,AND THE WAVEDYMFOAM SOLVER DOMAIN, Γ

2.RESULTS

The two-dimensional numerical wave tank is depicted in Figure 3, and emulates the numerical simulation based on potential flow theory described in Koo et al.[24].

The moored floating body is placed at the center of the numerical domain. The water depth is equal to the wave length. The depth of the air zone is half of the water depth. The lengths of wave generation and wave absorption zones vary based on the specific load case. However, the length should be relatively long to limit any wave reflection from the boundary.

TABLE 1: FLOATING BODY STRUCTURAL CHARACTERISTICS

Mass(kg)	125
Moment of inertia about the gravitational center(kg·m^2)	4.05
Width(m)	0.5
Draft(m)	0.25
Local radius of round corner(m)	0.064
Gravitational center above the keel (m)	0.135

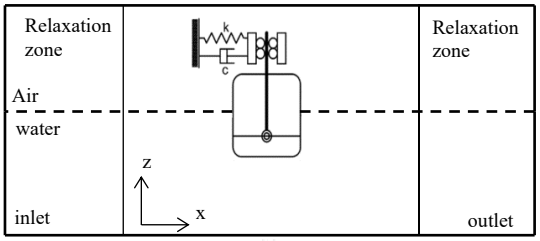

FIGURE 3: OVERVIEW OF THE NUMERICAL SIMULATION SET-UP

The characteristics of the body are presented in Table 1. The mooring line is modelled by a horizontal spring through the gravitational center with the spring stiffness taken as 197.58 N/m and the damping coefficient taken as 19.8 N/m/s. The body moves in surge (x), heave (z) and pitch directions.

Figure 3 shows that the spring only imposes a constraint in the surge direction, no constraint in heave direction. For the numerical model in OpenFOAM, the spring constraint is implemented based on the attachment point and anchor point, which means the spring will constrain the heave motion. In order to reduce this effect, the anchor point is 100 m away from the attachment point in the numerical model. To verify the numerical model, heave decay tests with and without spring were carried out, as shown in Figure 4. Due to the small heave motion relative to the length of spring, the spring has no influence on heave motion. which means the numerical model is the same as the model in [22].

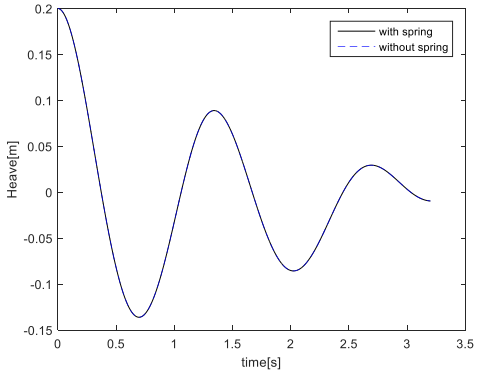

FIGURE4: TIME SERIES OF HEAVE DECAY TESTS WITH AND WITHOUT SPRING

2.1 FREE DECAY TESTS

To analyze and compare the unforced response of the moored floating body in surge, heave and pitch, free decay tests are carried out. The length of wave generation and absorption zones is 4 m and the center of body is 6 m away from the inlet boundary. The time series of the heave motion with different refinement levels are presented in Figure 5. The cell size is defined by the number of points per structure length (p.p.s.l), where the characteristic length is 0.5 m in this case.

Figure 5 shows firstly that the numerical solutions don't diverge. Secondly, after two natural periods, the damping for the higher resolution is larger than that with lower resolution. The natural periods for different spatial discretisations are not the same, as presented in Table 2. The reason can be found in the nonlinearities or vortices that are captured by the mesh. Considering the small error between low level and high level of mesh refinement, the background mesh resolution (30 p.p.s.l) is used for the remainder of the simulations.

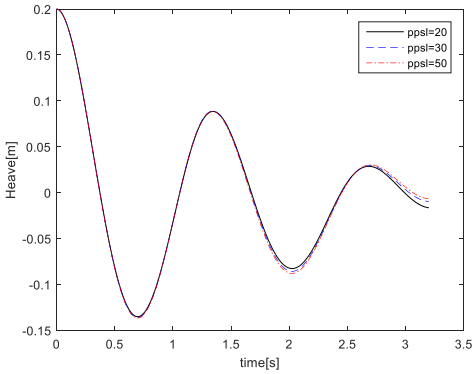

FIGURE 5: TIME SERIES OF HEAVE DECAY TEST WITH DIFFERENT SPATIAL DISCRETISATIONS

TABLE 2: COMPARISON OF HEAVE NATURAL PERIOD FOR DIFFERENT SPATIAL DISCRETISATIONS

Spatial discretisation (p.p.s.l)	Natural period(s)
20	1.362
30	1.365
50	1.365

The surge and pitch natural periods (Table 3) can be found through free decay tests in the surge and pitch directions with background mesh resolution of 30 p.p.s.l.

TABLE 3: NATURAL PERIODS IN SURGE AND PITCH

Degree of freedom	Natural period (s)
Surge	7.289
Pitch	1.427

2.2 RESULTS AND ANALYSIS OF REGULAR WAVE CASE

In this section, the motions and loads of the body under a regular wave are presented and analyzed.

2.2.1 WAVE PROPAGATION

In the numerical simulation, the wave is generated based on stream function wave theory [25]. The outlet boundary is defined by setting a constant current with zero velocity. The generated

wave includes a ramping-up stage. The numerical domain is the same as that used in the free decay test except the length of wave absorption zone is 8 m. The generated wave parameters are presented in Table 4.

TABLE 4: WAVE PARAMETERS OF REGULAR WAVE

Wave period(s)	1.158
Wave height(m)	0.07
Water depth(m)	2
Wave steepness	0.033
Fourier modes	32

The time series of surface elevation at the center of body with different spatial discretisations are compared to the analytical stream function solution in Figure 6. The wave amplitude decreases with the lower level of mesh refinement. The reason for this is the surface smearing, ever though this effect has been reduced by including the additional convective term in Equation (6). The wave amplitude of mesh resolution of 20 p.p.s.l and 30 p.p.s.l is respectively 11.6% and 3.6% smaller than that of mesh resolution of 50 p.p.s.l. The background mesh resolution of 30 p.p.s.l was adopted to decrease the computational cost and applied for the rest of the simulations. In order to get the accurate wave elevation at the center of body, the wave amplitude at the inlet was adjusted to make sure that the wave amplitude of 30 p.p.s.l is the same as the analytical solution before the body is put into the numerical domain. That is the reason that the measured wave elevation of the finest mesh (50 p.p.s.l) is larger than the analytical solution.

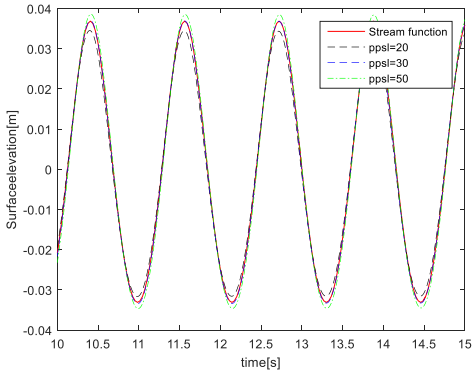

FIGURE 6: TIME SERIES OF WAVE ELEVATIONS WITH DIFFERENT SPATIAL DISCRETISATIONS

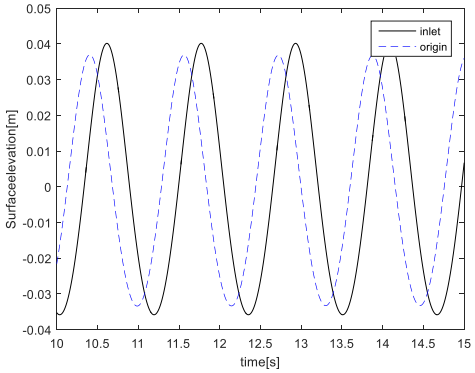

FIGURE 7: COMPARISON OF TIME SERIES OF WAVE ELEVATIONS AT INLET AND AT THE CENTER OF BODY (30 p.p.s.l)

Figure 7 compares the wave amplitude at the inlet boundary and at the center of the body. The decrease in amplitude is caused by numerical diffusion. Another observation is that the amplitude of wave peak is larger than that of wave trough. That implies that the nonlinear terms show up in the time series of surface elevation.

2.2.2 FLOW-INDUCED MOTIONS

Figure 8a, 8b and 8c present the motions of the moored floating body under the regular wave from 40 s to 60 s. The previous data is discarded to avoid the initial impact on the body.

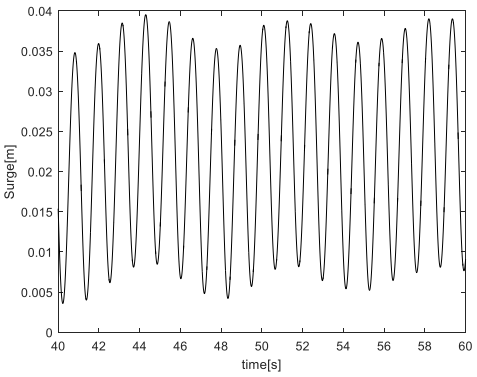

a) SURGE RESPONSE

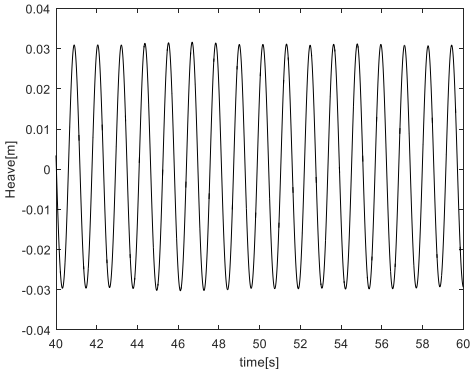

b) HEAVE RESPONSE

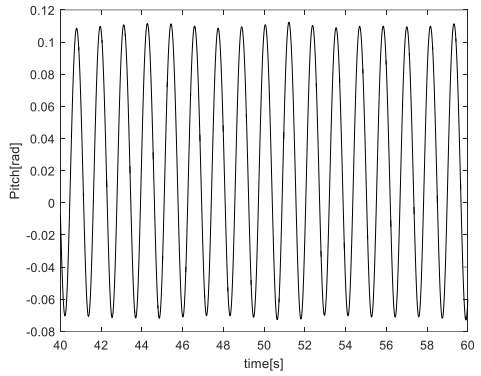

c)PITCH RESPONSE

FIGURE 8: MOTION RESPONSE OF MOORED FLOATING BODY UNDER REGULAR WAVE

Due to small damping in the surge direction, the steady state is not reached until the end of simulation. A non-zero mean surge motion, caused by wave drift force, is observed in numerical results. Meanwhile, a non-zero mean pitch angle, caused by a mean pitch moment, also exists in numerical results. These three degrees of freedom oscillate with the same period (around 1.165 s), which is slightly different from wave period (1.158 s). This can be explained by the effect of the drift motion.

The comparisons of the amplitude of body motion are presented in Table 5. The height of body motion is the mean of the peak-to-peak total height of the numerical response in the respective direction. The results of linear analysis and fully nonlinear analysis based on potential flow theory are from Koo et al [22]. It can be concluded that the potential-based numerical method overpredicts response compared to CFD.

TABLE 5: COMPARISON OF BODY MOTION RESPONSE WITH DIFFERENT METHODS UNDER REGULAR WAVE FROM TABLE 4.

Degree of freedom	CFD	Linear analysis [22]	Fully nonlinear analysis [22]
Surge(m)	0.0309	0.0357	0.0336
Heave(m)	0.0608	0.0679	0.0644
Pitch(rad)	0.1815	0.1617	0.1816

2.2.3 FLOW-INDUCED LOADS

Figure 9a, 9b and 9c present the flow-induced loads on the moored floating body under the regular wave from 40 s to 60 s. The moment is about the center of mass of body.

It can be observed that there is a non-zero mean value for the surge force and pitch moment and buoyancy is included in heave force. Besides the wave frequency, there is another frequency in the pitch moment which is close to the surge natural frequency. That means the pitch moment is affected by the surge motion.

From Figure 10, which is a zoomed version of Figure 9a), only minor disturbance can be observed when the maximum body motion is achieved, which means under-relaxation method or predictor-corrector method is able to provide a stable solution.

To show the effect of nonlinearity on the wave loads, the flow-induced load from CFD is compared to the 1st order load from Koo et al [22], which is presented in Table 6. The height of the flow-induced load is computed as the mean of the peak-to-peak total height of the load response in the respective direction. For the surge force, the 1st order load is dominant, while for the heave force and pitch moment, the nonlinear wave loads are more important. The nonlinear loads mainly come from the change of wetted body surface, the change of normal direction of body surface, the nonlinear terms in pressure and so on. Note that the velocity-squared term in pressure will reduce the total flow-induced load.

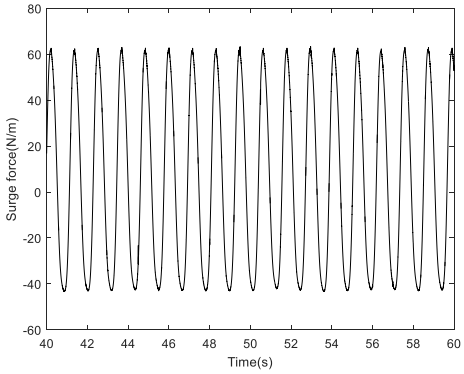

a) SURGE FORCE

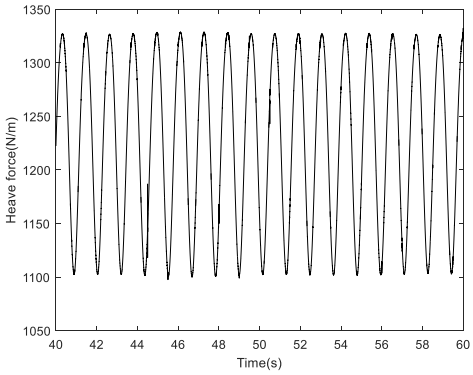

b) HEAVE FORCE

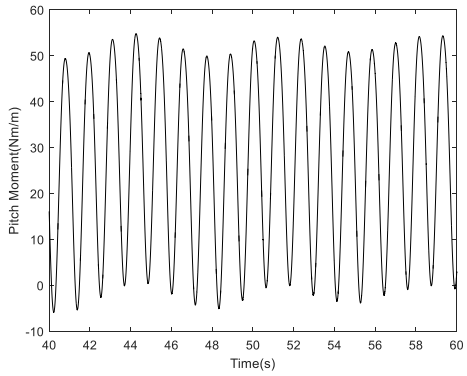

c) PITCH MOMENT

FIGURE 9: FlOW-INDUCED LOADS ON MOORED FLOATING BODY UNDER REGULAR WAVE FROM TABLE 4.

Table 6: COMPARISON OF DYNAMIC FLOW-INDUCED LOADS WITH DIFFERENT METHODS UNDER REGULAR WAVE FROM TABLE 4. HEIGHT (DOUBLE-AMPLITUDE) IS SHOWN.

Degree of freedom	CFD	1st order load
Surge force (N/m)	105.15	120.68
Heave force (N/m)	224.89	127.30
Pitch Moment (Nm/m)	54.35	23.28

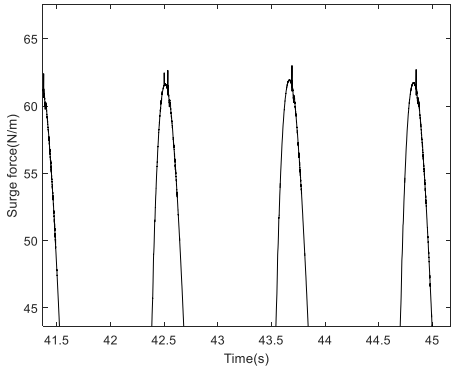

FIGURE 10: ZOOM OF FIGURE 9 a)

2.3 RESULTS AND ANALYSIS OF IRREGULAR WAVE CASE

In this section, the motions and loads of the body under irregular waves are presented and analyzed.

2.3.1 WAVE PROPAGATION

In the numerical simulation, the wave is generated based on a Jonswap wave spectrum in Oceanwave3D. The outlet boundary is defined by setting a constant current with zero velocity. The generated wave also includes a ramping-up stage. The length of potential flow solver is 16 m and the length of Navier-Stokes/VOF solver is 4 m. The center of the two solvers is located at the same position. The length of relaxation zone of Navier-Stokes/VOF solver is 1 m. The spatial discretization in the Navier-Stokes/VOF solver is the same as that used in the regular wave case. The cell size in potential flow solver is 10 times larger than that in Navier-Stokes/VOF solver. The parameters of the wave spectrum are given in Table 7.

TABLE 7: IRREGULAR WAVE PARAMETERS

Significant wave height (m)	0.0368
Wave peak period (s)	1.158
Peak enhancement factor γ	3.3

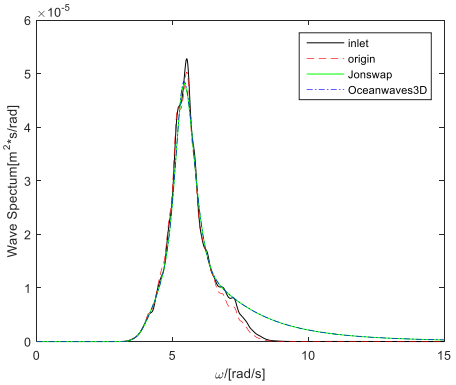

FIGURE 11: COMPARISON OF WAVE SPECTURM

Based on the time series of surface elevation from 400s to 4000s, the wave spectra at inlet and origin of Navier-stokes/VOF solver are given in Figure 11, which is compared to the wave spectrum input in Oceanwave3D and the theoretical Jonswap wave spectrum. The wave spectrum input in Oceanwave3D is the same as the theoretical Jonswap wave spectrum. The potential flow solver determines a cut-off frequency based on the Nyquist frequency, so the wave spectrum is truncated for the higher frequencies, which can be observed from Figure 11. Furthermore, the generated wave has more energy in the wave frequency. Another observation is that due to numerical effects, the wave energy decreases as the wave propagates.

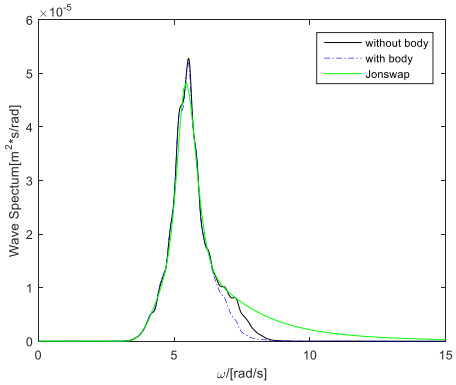

FIGURE 12: COMPARISON OF WAVE SPECTURM AT INLET WITH AND WITHOUT BODY

When the body is placed in the numerical domain, considering the small relaxation zone, the reflected wave is not fully absorbed by the relaxation zone and reduces the wave energy in high frequencies at the inlet of Navier-Stokes/VOF solver, which is shown in Figure 12. The simplest solution to exclude this disturbance would be to use a longer domain, but this will increase computational costs.

2.3.2 FLOW-INDUCED MOTIONS

The body motion power spectra for irregular waves are made based on the 1 h (from 400 s to 4000 s) time domain simulation in CFD, which are shown in Figure 13.

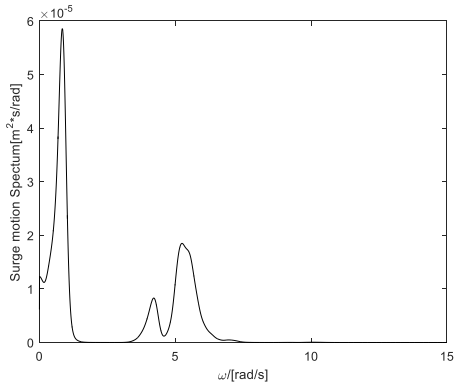

a) SURGE MOTION SPECTRUM

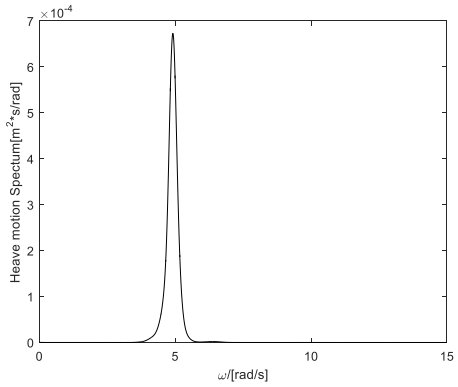

b) HEAVE MOTION SPECTRUM

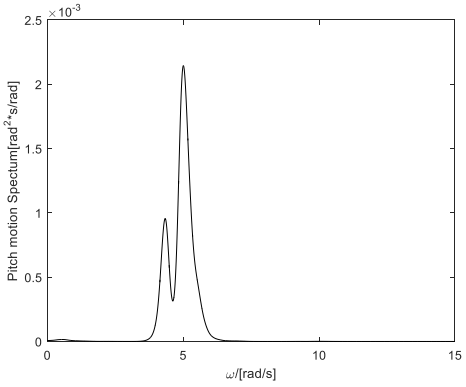

c) PITCH MOTION SPECTRUM

FIGURE 13: MOORED FLOATING BODY MOTION SPECTRA UNDER IRREGULAR WAVE FROM TABLE 7.

It can be seen that for the surge motion, the flow-induced response is mainly concentrated at the surge natural frequency. The amplitude of the flow-induced response at the wave frequency is small. In addition, the flow-induced loads also stimulate a response around the pitch natural frequency. This can indicate the body pitches about a point that is not at the center of mass of body and the coupling between surge and pitch motion. The heave natural frequency is close to the wave frequency and difference between the amplitudes of response around these two frequencies is quite small, so when smoothing the profile of heave motion spectrum, the peaks at the wave and natural frequency merge into one peak. For the pitch motion, responses appear around the pitch natural frequency and wave frequency. The differences among the peak frequencies and wave frequency, pitch natural frequency and heave natural frequency can be explained by the drift motion of body.

In Table 8, the statistical results of body motion in the surge, heave and pitch direction are summarized. It is also found that as in the regular wave case, there are nonzero mean surge and pitch motions.

Table 8: STATISTICAL RESULTS OF BODY MOTION UNDER THE IRREGULAR WAVE FROM TABLE 7.

	Surge(m)	Heave(m)	Pitch(rad)
Maximum value	0.0399	0.0682	0.1581
Mean value	0.0059	0	0.0027
Minimum value	-0.0209	-0.0688	-0.1594
Standard deviation	0.0075	0.0169	0.0400

2.3.3 FLOW-INDUCED LOADS

Figure 14 presents the power spectra of the force and moment on the moored floating body for irregular wave based on the 1 h (from 400 s to 4000 s) time domain simulation in CFD.

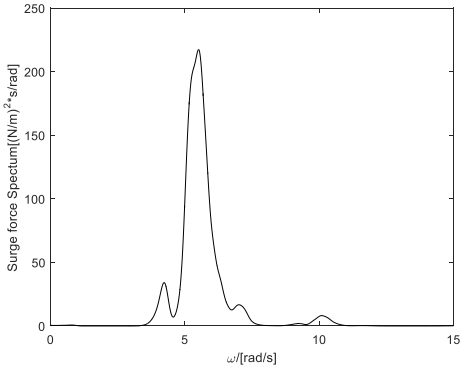

a) SURGE FORCE SPECTRUM

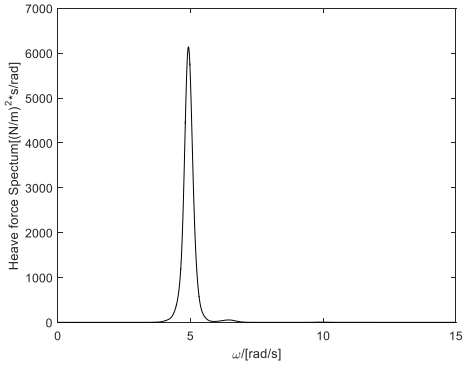

b) HEAVE FORCE SPECTRUM

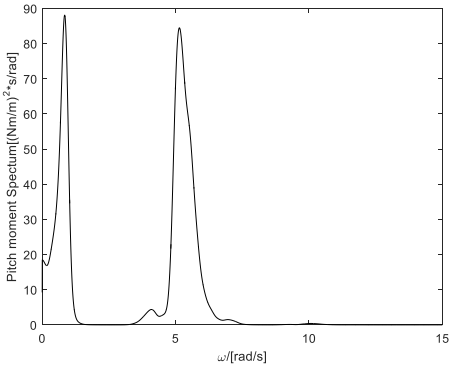

c)PITCH MOMENT SPECTRUM

FIGURE 14: MOORED FLOATING BODY LOAD SPECTRA

The flow-induced surge force is mainly concentrated at the wave frequency. Furthermore, there is also a small load around the pitch natural frequency. This also indicates that the pitch motion has small influence on the surge force. For the heave force, due to the same reason as the heave motion spectrum, two different peaks merge into one peak after smoothing the profile of heave force spectrum. For the pitch moment, the loads act at both the surge natural frequency and the wave frequency. However, around pitch natural frequency, the amplitude of the load is quite small. Another observation is that loads around the double wave frequency exist in all load spectra, which is caused by the sum-frequency effects.

In Table 9, the statistical results of body loads are summarized. As in the regular wave case, there are nonzero mean surge forces and pitch moments.

TABLE 9: STATISTICAL RESULTS OF BODY LOADS UNDER IRREGULAR WAVE FROM TABLE 7. NOTE THAT THE HEAVE FORCE INCLUDES HYDROSTATIC PRESSURE.

	Surge force (N/m)	Heave force (N/m)	Pitch Moment (Nm/m)
Maximum value	68.8631	1426.4	56.7516
Mean value	1.1667	1226.3	7.2433
Minimum value	-65.5931	989.0	-30.9232
Standard deviation	15.5905	51.157	10.8434

3. SUMMARY

This study deals with the motion and force response of a moored floating 2D body under regular and irregular wave conditions using high-fidelity simulation tool OpenFOAM. The results are compared against the results from linear and fully nonlinear analysis based on potential flow theory.

To verify the generated waves, simulations without the body are carried out. Due to numerical diffusion, the wave amplitude of regular wave at the inlet must be adjusted in order to obtain the desired wave. The time series of wave elevation at the body show the expected nonlinear characteristics.

Further, this numerical tank is used for simulations of a moored floating 2D body subjected to regular and irregular waves. Coupling is observed in the motions and forces between surge and pitch directions. Compared to potential flow theory results, the amplitude of the motion response is reduced.

Even though the numerical model can compute the dynamic motion and force response of a moored floating body, further improvement is still required to solve the minor numerical disturbance when the maximum body motion response is achieved. There is still a need for more rigorous validation of the irregular wave cases, and application of the method to more complex floating structures for offshore wind.

ACKNOWLEDGEMENTS

The author Haoran Li gratefully acknowledges the financial support from China Scholarship Council (CSC). The discussions with Irene Rivera-Arreba (TU Delft) are greatly appreciated.

REFERENCES

[1] Wu G X, Taylor R E. The coupled finite element and boundary element analysis of nonlinear interactions between waves and bodies[J]. Ocean Engineering, 2003, 30(3): 387-400.

[2] Bouscasse B, Colagrossi A, Marrone S, et al. Nonlinear water wave interaction with floating bodies in SPH[J]. Journal of Fluids and Structures, 2013, 42: 112-129.

[3] Lee C H, Newman J N. First-and second-order wave effects on a submerged spheroid[J]. 1991.

[4] Celebi M S. Fully nonlinear 3-D numerical wave tank simulation[J]. JOURNAL OF SHIP RESEATCH, 1997, 42: 33-45.

[5] Kashiwagi M. Full-nonlinear simulations of hydrodynamic forces on a heaving two-dimensional body[J]. Journal of the Society of Naval Architects of Japan, 1996, 1996(180): 373-381.

[6] Kim M H, Celebi M S, Kim D J. Fully nonlinear interactions of waves with a three-dimensional body in uniform currents[J]. Applied Ocean Research, 1998, 20(5): 309-321.

[7] Ma Q W, Wu G X, Eatock Taylor R. Finite element simulations of fully non-linear interaction between vertical cylinders and steep waves. Part 2: numerical results and validation[J]. International Journal for Numerical Methods in Fluids, 2001, 36(3): 287-308.

[8] Wu G X, Taylor R E. Time stepping solutions of the two-

dimensional nonlinear wave radiation problem[J]. Ocean Engineering, 1995, 22(8): 785-798.
[9] Yu Y H, Li Y. Reynolds-Averaged Navier–Stokes simulation of the heave performance of a two-body floating-point absorber wave energy system[J]. Computers & Fluids, 2013, 73: 104-114.
[10] Verduzco-Zapata M, Ocampo-Torres F. Study of a 6 DOF wave energy converter interacting with regular waves using 3D CFD[C]//Proceedings of the 11th European Wave and Tidal Energy Conference. 2015: 1-6.
[11] Bhinder M A, Babarit A, Gentaz L, et al. Potential time domain model with viscous correction and CFD analysis of a generic surging floating wave energy converter[J]. International Journal of Marine Energy, 2015, 10: 70-96.
[12] Weller H G, Tabor G, Jasak H, et al. A tensorial approach to computational continuum mechanics using object-oriented techniques[J]. Computers in physics, 1998, 12(6): 620-631.
[13] Jacobsen N G, Fuhrman D R, Fredsøe J. A wave generation toolbox for the open-source CFD library: OpenFoam®[J]. International Journal for Numerical Methods in Fluids, 2012, 70(9): 1073-1088.
[14] Paulsen B T, Bredmose H, Bingham H B, et al. Forcing of a bottom-mounted circular cylinder by steep regular water waves at finite depth[J]. Journal of fluid mechanics, 2014, 755: 1-34.
[15] Hirt C W, Nichols B D. Volume of fluid (VOF) method for the dynamics of free boundaries[J]. Journal of computational physics, 1981, 39(1): 201-225.
[16] Sen D. A numerical method for two-dimensional studies of large amplitude motions of floating bodies in steep waves[D]. Memorial University of Newfoundland, PhD thesis,1988.
[17] Bruinsma N. Validation and application of a fully nonlinear numerical wave tank[D]. Delft University of Technology, master's thesis,2016.
[18] Bos F M, van Oudheusden B W, Bijl H. Radial basis function based mesh deformation applied to simulation of flow around flapping wings[J]. Computers & Fluids, 2013, 79: 167-177.
[19] Causin P, Gerbeau J F, Nobile F. Added-mass effect in the design of partitioned algorithms for fluid–structure problems[J]. Computer methods in applied mechanics and engineering, 2005, 194(42-44): 4506-4527.
[20] Dunbar A J, Craven B A, Paterson E G. Development and validation of a tightly coupled CFD/6-DOF solver for simulating floating offshore wind turbine platforms[J]. Ocean Engineering, 2015, 110: 98-105.
[21] Ferziger J H, Peric M. Computational methods for fluid dynamics[M]. Springer Science & Business Media, 2012.
[22] Engsig-Karup A P, Bingham H B, Lindberg O. An efficient flexible-order model for 3D nonlinear water waves[J]. Journal of computational physics, 2009, 228(6): 2100-2118.
[23] Paulsen B T, Bredmose H, Bingham H B. An efficient domain decomposition strategy for wave loads on surface piercing circular cylinders[J]. Coastal Engineering, 2014, 86: 57-76.
[24] Koo W, Kim M H. Freely floating-body simulation by a 2D fully nonlinear numerical wave tank[J]. Ocean Engineering, 2004, 31(16): 2011-2046.
[25] Fenton J D. The numerical solution of steady water wave problems[J]. Comp. Geosci., 1988, 14(3): 357-368.